Analysis of the Electrolytic Codeposition of Non-Brownian Particles with Metals

J. Fransaer, J. P. Celis, and J. R. Roos*

Department of Metallurgy and Materials Engineering, Katholieke Universiteit Leuven, de Croylaan 2, B-3001 Heverlee, Belgium

ABSTRACT

A model for the electrolytic codeposition of spherical particles with metals on a rotating disk electrode is presented, based on a trajectory analysis of the particle deposition, including convective mass transport, geometrical interception, and migration under specific forces, coupled to a surface immobilization reaction. A number of relevant forces were included and their effects determined. Theoretical predictions of this model are compared with experimental results for the codeposition of spherical polystyrene particles with copper during electrolysis from an acid copper sulfate solution. The influence of fluid flow velocities, particle concentration, and current density on the rate of particle deposition is illustrated. Experiments done on a rotating disk electrode allow the adhesion forces to be determined from the distribution of particles on the surface. It is shown that codeposition is governed by colloidal interactions that can, in first order, be approximated by the Derjaguin-Landau-Verwey-Overbeek interactions plus an additional short range repulsion that was associated with the hydration force.

The entrapment of ceramic, polymer, and metal powders suspended in an electroplating bath during metal electrodeposition is a process called electrolytic codeposition or composite plating. The simultaneous deposition of particles and metal brings about interesting changes in physical and mechanical properties of the coatings (1). Recently, it has been found that the electrolytic codeposition of liquid-containing microcapsules enables the production of self-lubricating coatings through the inclusion of oil (2). The codeposition of polymer particles provides an excellent adhesion of paint or plastic top coatings. The synthesis of these new coatings has spurred considerable industrial interest. Despite the growing number of applications, the underlying physics of the codeposition process have eluded systematic analysis. One of the first attempts to describe the mechanism of electrolytic codeposition is the pioneering work of Guglielmi (3). But the state of modeling is still far from the ultimate goal, being the prediction of the rate of particle codeposition.

The deposition of particles in other industrial processes, such as deep-bed filtration, flotation, and fouling, has led to a growing body of experimental and theoretical investigations on the mechanism of particle deposition (4-6). However, the link to the field of electrolytic codeposition has never been made, nor has it been shown that the trajectory description can be useful in the context of electrolytic codeposition. The most pronounced difficulties in the transfer of knowledge between the area of filtration and electrolytic codeposition are obvious; filtration deals with dilute solutions, rarely more concentrated than 10^{-2} molar, with a low particle concentration. Furthermore, in codeposition the collector is not a dielectric but a metal electrode. In fact, the electrolytic codeposition of particles proceeds under nonequilibrium conditions and is accompanied by a flow of ions across the electrode, the progressive development of a surface texture and a roughening of the deposit during electrodeposition.

Two factors that have further plagued the theoretical progress and have led to considerable confusion lie in the nature of codeposition experiments carried out so far. Most codeposition experiments deal with mineral particles, irregularly shaped, with jagged edges; the result of grinding or milling, having irreproducible charge distributions and an unknown surface chemistry. The incomplete and sketchy information on such systems may explain the contradictory data reported on electrolytic codeposition. The irregular shape and properties also made the theoretical modeling more complex as most theories about particle-wall interactions assume spherically shaped, isotropic particles on a flat surface. Furthermore, most of the early work on electrolytic codeposition was carried out on stationary plane electrodes in cells, where the particles were kept in suspension by gas bubbling or vibrating perforated bottom plates. Therefore, due to the ill-defined and poorly reproducible hydrodynamical plating conditions, comparison of literature data is difficult. This is especially true since the electrolytic codeposition process is strongly affected by the hydrodynamical conditions prevailing in the vicinity of the cathode.

Two basic questions await explanation in analyzing the codeposition of particles from aqueous plating baths. Upon arrival at the cathode, a particle must, somehow, stick to the surface, otherwise it will not contribute to the electrolytic codeposition. How does a particle become captured from the plating bath and what are the forces responsible for this? On the other hand, not all particles reaching the electrode surface will necessarily be trapped. Consequently, some of the particles that come into contact with the electrode detach again. What is the force required to release the deposited particulate material?

It should be pointed out that the specific surface interactions during codeposition should be viewed as dynamic rather than static. Since codeposition of particles takes place on a renewable (growing) surface, time is an important variable. The continuous buildup of metal influences the geometry of the electrode, especially the area of the electrode in closest contact with the particle, thus changing the initial particle-electrode interaction with time.

The aim of this paper is to present a theoretical framework in which electrolytic codeposition experiments of non-Brownian particles can be analyzed. For this purpose, the trajectory analysis is used as a starting point.

The Trajectory Equation for Large Particles around a RDE

Based on the knowledge of the flow field around an electrode, and taking into account all the forces acting on a particle, the trajectory of that particle can be determined from the equation of motion. If a criterion of particle attachment, once in contact with the electrode, is assumed (the most simple one would be that all particles stick to the electrode upon contact), it becomes possible to determine the codeposition rate. The forces acting on a particle can be divided into forces exerted by the fluid on the particle due to the convection of the fluid and the motion of the particle in the fluid, and forces that act on the particle itself, such as gravity, buoyancy, and other body forces. The various fluid forces that act on a particle are schematically shown in Fig. 1. If the particle is large (>1 μm), its Brownian motion may be neglected and the momentum balance on the particle suffices for predicting the particle trajectory. As long as the particle concentration is low and the particle size is much smaller than the rotating disk electrode (RDE) and the thickness of the hydrodynamical boundary layer, it is possible to make the following assumptions about the motion of particle and fluid; the flow

* Electrochemical Society Active Member.

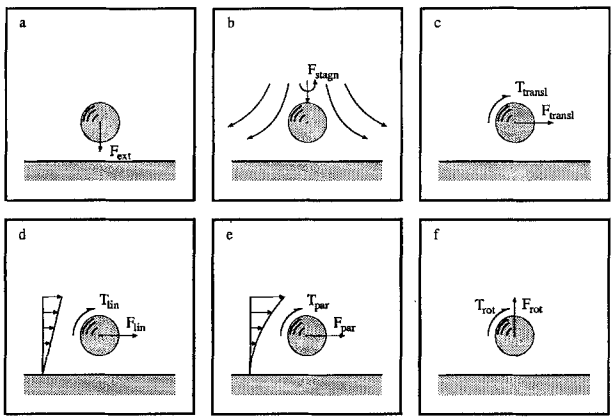

Fig. 1. Various hydrodynamic forces acting on a particle near an electrode: a: Particle moving normal to the surface under the influence of an external force, b: Stationary particle in stagnation point flow, c: Particle moving parallel to the surface, d: Stationary particle in a linear shear flow, e: Stationary particle in a quadratic (parabolic) shear flow, f: Particle rotating around an axis parallel to the surface.

field is undisturbed by the presence of particles, except in the immediate vicinity of a particle, and, when a particle is more than several particle diameters away from the electrode, the particle center moves along undisturbed fluid streamlines.

To derive the expressions for the hydrodynamical corrections to the motion of a particle in the vicinity of a plane surface, the Navier-Stokes equations for the flow disturbance $\hat{\mathbf{v}}$ around a particle moving with a characteristic linear velocity $\mathbf{u}$ and rotational velocity Ω, need to be solved

$$\nabla^2\hat{\mathbf{v}} - \nabla p = \mathrm{Re}\left[\frac{\partial\hat{\mathbf{v}}}{\partial t} + (\hat{\mathbf{v}}\cdot\nabla)\cdot\hat{\mathbf{v}}\right] \qquad [1]$$

where p is the dynamic pressure, Re is the Reynolds number, and t is the time. As boundary conditions, the undisturbed flow field far from the particle and the no-slip boundary conditions on the surface of the particle and disk, are taken. The translational velocities of the particles entrained by the fluid are small (relative to the fluid) and the Reynolds number is based on the spherical particle with radius a_p

$$\mathrm{Re} = \frac{2a_p|\mathbf{u}-\mathbf{v}|}{\nu} \qquad [2]$$

where ν is the kinematic viscosity, is much smaller than unity. Using the above information Eq. [1] reduces to the creeping motion equations

$$\nabla^2\hat{\mathbf{v}} = \frac{1}{\mu}\nabla p \qquad [3a]$$

$$\nabla\cdot\hat{\mathbf{v}} = 0 \qquad [3b]$$

where $\mu = \nu/\rho$ equals the absolute fluid viscosity and ρ is the density of the fluid. In the case of a rotating disk, the fluid flow velocity $\mathbf{v}$ close to the disk is given by the well-known Navier-Stokes solution (7)

$$\mathbf{v} = r\omega\sum_{n=0}^{\infty} f_n\zeta^n\mathbf{i}_r + r\omega\sum_{n=0}^{\infty} g_n\zeta^n\mathbf{i}_\theta + \sqrt{\omega\nu}\sum_{n=0}^{\infty} h_n\zeta^n\mathbf{i}_z \qquad [4]$$

where $\zeta = \sqrt{\omega/\nu}\,z$ and ω is the angular velocity of the disk. The above velocity field in turn can be written as a Taylor expansion around the instantaneous position of the particle center (r_p, θ_p, z_p), in a local cartesian coordinate system (x, y, z), in which the unit vectors $\mathbf{i}_x$, $\mathbf{i}_y$, and $\mathbf{i}_z$ coincide with the directions of the unit vectors $\mathbf{i}_r$, $\mathbf{i}_\theta$, and $\mathbf{i}_z$ [Fig. 2]

Table I. Values of parameters used in the trajectory calculation.

$r_D = 1.5\times10^{-2}$ m	$\epsilon_r = 2.49 - 2.55$
$a_p = 11$ μm	$T = 296$ K
$\rho_p = 1.04 + 1.065$ kg dm^{-3}	$E_{pzc} = 115$ mV
$\rho_f = 1.1$ kg dm^{-3}	$\zeta_p = 13.5$ mV

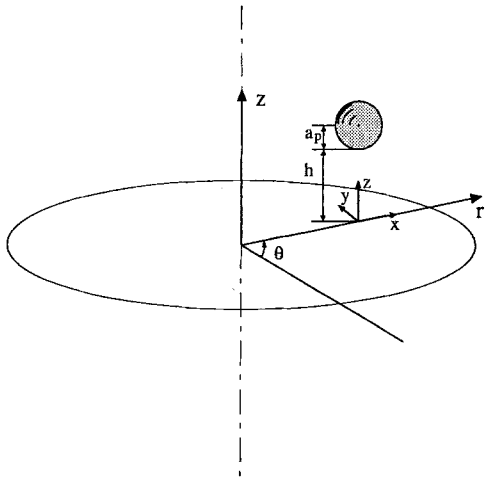

Fig. 2. Perspective drawing of the various coordinates used in the description of the trajectory analsyis.

$$\mathbf{v} = \left\{(r_p + x)\omega\sum_{n=0}^{\infty} f_n\zeta^n - y\omega\sum_{n=0}^{\infty} g_n\zeta^n\right\}\mathbf{i}_x$$

$$+\left\{(r_p + \omega)\omega\sum_{n=0}^{\infty} g_n\zeta^n + y\omega\sum_{n=0}^{\infty} f_n\zeta^n\right\}\mathbf{i}_y$$

$$+\sqrt{\omega\nu}\sum_{n=0}^{\infty} h_n\zeta^n\mathbf{i}_z \qquad [5]$$

Near the disk, ζ is small and the flow field relative to the disk is well approximated by retaining only second order terms in x, y, and z

$$\mathbf{v} = \left\{f_1\frac{\omega^{3/2}}{\nu^{1/2}}r_p z + f_1\frac{\omega^{3/2}}{\nu^{1/2}}xz - g_1\frac{\omega^{3/2}}{\nu^{1/2}}yz - \frac{\omega^2}{2\nu}r_p z^2\right\}\mathbf{i}_x \qquad [6a]$$

$$+\left\{g_1\frac{\omega^{3/2}}{\nu^{1/2}}r_p z + g_1\frac{\omega^{3/2}}{\nu^{1/2}}xz + f_1\frac{\omega^{3/2}}{\nu^{1/2}}yz\right\}\mathbf{i}_y \qquad [6b]$$

$$-f_1\frac{\omega^{3/2}}{\nu^{1/2}}z^2\mathbf{i}_z \qquad [6c]$$

or regrouping terms

$$\mathbf{v} = f_1\frac{\omega^{3/2}}{\nu^{1/2}}\{xz\mathbf{i}_x + yz\mathbf{i}_y - z^2\mathbf{i}_z\} \qquad [7a]$$

$$+ f_1\frac{\omega^{3/2}}{\nu^{1/2}}r_p z\mathbf{i}_x + g_1\frac{\omega^{3/2}}{\nu^{1/2}}r_p z\mathbf{i}_y \qquad [7b]$$

$$-\frac{\omega^2}{2\nu}r_p z^2\mathbf{i}_x \qquad [7c]$$

$$+ g_1\frac{\omega^{3/2}}{\nu^{1/2}}\{xz\mathbf{i}_y + yz\mathbf{i}_x\} \qquad [7d]$$

In this way the local flow is decomposed into an axisymmetrical stagnation flow (Eq. [7a]), two linear shear flows (Eq. [7b]), one parabolic shear flow (Eq. [7c]) and a local rotation (Eq. [7d]). It is clear from symmetry considerations, that the rotational flow merely spins the particle

around an axis normal to the disk. For spherical particles this spin does not affect particle transport and will thus be discarded in the further analysis.

In view of the linearity of the creeping flow equations and the boundary conditions, the motion of the particle may be resolved into a radial (or tangential) contribution, an axial (or normal) component, and an angular component. The axial motion of a particle is further resolved in two hydrodynamic forces. The first, propelling the particle towards the disk, is exerted by the axisymmetric stagnation point flow on a fixed particle. This hydrodynamic force, designated F_{stagn}, was obtained by Goren and O'Neill (8)

$$\mathbf{F}_{stagn} = -6\pi\mu a_p^3 \nu_{stagn} \tilde{F}_{stagn} \mathbf{i}_z \qquad \text{with } \nu_{stagn} = f_1 \frac{\omega^{3/2}}{\nu^{1/2}} \qquad [8]$$

All forces and torques designated by the superscript ~ are normalized with respect to the Stokes force and torque, respectively $F_{Stokes} = 6\pi\mu a_p U$ and $T_{Stokes} = 8\pi\mu a_p^2 \Omega$, felt by a sphere of radius a_p either translating with velocity U or rotating with a steady angular velocity Ω in an unbounded fluid with viscosity μ. The second force is the resistance felt by a spherical particle moving perpendicular to the disk under the influence of an externally applied force, in an otherwise quiescent fluid

$$\mathbf{F}_\perp = 6\pi\mu a_p \frac{dz_p}{dt} \tilde{F}_\perp \mathbf{i}_z \qquad [9]$$

This force is function of the instantaneous normal velocity dz_p/dt of the particle (9). $\tilde{F}_\perp$ is the ratio of the particle velocity under an applied force normal to the electrode to that which the particle would have in an unbounded fluid under the same force. In both cases, due to the axial symmetry, the particle experiences only a force and no torque. Taking a force balance on the sphere, the hydrodynamical forces must match the external force at any instant along the particle trajectory $F_{ext} + F_{stagn} + F_\perp = 0$, which results in

$$\frac{dz_p}{dt} = a_p^2 \nu_{stagn} \frac{\tilde{F}_{stagn}}{\tilde{F}_\perp} - \frac{F_{ext}}{6\pi\mu a_p \tilde{F}_\perp} \qquad [10]$$

Similarly the radial motion of the particle near the rotating disk is obtained by setting up the momentum balance equations for the tangential forces and torques. Near the electrode the particle finds itself in two radially outwards directed flow fields, namely, a linear and a parabolic shear flow. The procedure for obtaining the force (**F**) and torque (**T**) exerted by a linear and parabolic shear flow on an immobile sphere in proximity to a plane wall, with no-slip boundary condition on both particle and RDE surface, was given by Goren and O'Neill (8)

$$\mathbf{F}_{lin} = 6\pi\mu a_p^2 \nu_{lin}^x \tilde{F}_{lin} \mathbf{i}_x \qquad \text{with } \nu_{lin}^x = f_1 \frac{\omega^{3/2}}{\nu^{1/2}} r_p \qquad [11a]$$

$$\mathbf{T}_{lin} = 8\pi\mu a_p^3 \nu_{lin}^x \tilde{T}_{lin} \mathbf{i}_y \qquad [11b]$$

$$\mathbf{F}_{par} = 6\pi\mu a_p^3 \nu_{par}^x \tilde{F}_{par} \mathbf{i}_x \qquad \text{with } \nu_{par}^x = -\frac{\omega^2}{2\nu} r_p \qquad [11c]$$

$$\mathbf{T}_{par} = 8\pi\mu a_p^4 \nu_{par}^x \tilde{T}_{par} \mathbf{i}_y \qquad [11d]$$

$\tilde{F}_{lin}$, $\tilde{T}_{lin}$, $\tilde{F}_{par}$, and $\tilde{T}_{par}$ are the ratios of the radially directed forces and torques that a stationary particle would experience near the electrode to that it would experience if held stationary in an unbounded fluid having the same flow field. To complete the description of the flow field, caused by the radial motion of a rigid sphere in the presence of a rigid plane, the forces and torques arising from the translational and rotational motion of a sphere near a plane wall in a fluid at rest at infinity have to be added. The solutions for a rigid sphere rotating with steady angular velocity Ω were given by O'Neill (10)

$$F_{rot} = 6\pi\mu a_p^2 \Omega \tilde{F}_{rot} \quad \text{and} \quad T_{rot} = 8\pi\mu a_p^3 \Omega \tilde{T}_{rot} \qquad [12]$$

while Dean and O'Neill (11) affected the exact bipolar solution of a particle translating with velocity U parallel to a plane interface

$$F_{transl} = 6\pi\mu a_p U \tilde{F}_{transl} \quad \text{and} \quad T_{transl} = 8\pi\mu a_p^2 U \tilde{T}_{transl} \qquad [13]$$

The only external force acting radially to the disk is the centrifugal force F_{centr} felt by the particle with mass m due to the rotation of the disk with angular velocity $d\theta_p/dt$ corrected for buoyancy

$$\mathbf{F}_{centr} = m r_p \left(\frac{d\theta_p}{dt}\right)^2 \mathbf{i}_x = \frac{4}{3} \pi a_p^3 (\rho_p - \rho_f) r_p \left(\frac{d\theta_p}{dt}\right)^2 \mathbf{i}_x \qquad [14]$$

From the momentum balance, written in terms of the nondimensional force and torque components

$$a_p \nu_{lin}^x \tilde{F}_{lin} + a_p^2 \nu_{par}^x \tilde{F}_{par} + a_p \Omega_r \tilde{F}_{rot} + U_r \tilde{F}_{transl} + \frac{F_{centr}}{6\pi\mu a_p} = 0 \qquad [15a]$$

$$a_p \nu_{lin}^x \tilde{T}_{lin} + a_p^2 \nu_{par}^x \tilde{T}_{par} + a_p \Omega_r \tilde{T}_{rot} + U_r \tilde{T}_{transl} = 0 \qquad [15b]$$

the translational (U_r) and rotational velocities (Ω_r) in the radial direction can be derived

$$\Omega_r = \frac{U_r}{a_p} \frac{\tilde{T}_{transl}}{\tilde{T}_{rot}} - \nu_{lin}^x \frac{\tilde{T}_{lin}}{\tilde{T}_{rot}} - a_p \nu_{par}^x \frac{\tilde{T}_{par}}{\tilde{T}_{rot}} \qquad [16a]$$

$$U_r = \frac{dr_p}{dt} \qquad [16b]$$

$$= \frac{F_{centr}}{6\pi\mu a_p} \frac{\tilde{T}_{rot}}{\tilde{F}_{rot}\tilde{T}_{transl} - \tilde{F}_{transl}\tilde{T}_{rot}} + a_p \nu_{lin}^x \frac{\tilde{F}_{lin}\tilde{T}_{rot} - \tilde{F}_{rot}\tilde{T}_{lin}}{\tilde{F}_{rot}\tilde{T}_{transl} - \tilde{F}_{transl}\tilde{T}_{rot}} + a_p^2 \nu_{par}^x \frac{\tilde{F}_{par}\tilde{T}_{rot} - \tilde{F}_{rot}\tilde{T}_{par}}{\tilde{F}_{rot}\tilde{T}_{transl} - \tilde{F}_{transl}\tilde{T}_{rot}} \qquad [16c]$$

Along the same line of reasoning, the angular trajectory motion can be found from the remaining y-directed shear flow, coupled to the translational and rotational disturbance flow fields. When the RDE rotates at a constant rotation speed, no angular force is present, and the angular motion of the particle and its accompanying fluid motion are not affected by external forces

$$a_p \nu_{lin}^y \tilde{F}_{lin} + a_p \Omega_\theta \tilde{F}_{rot} + U_\theta \tilde{F}_{transl} = 0 \qquad \text{with } \nu_{lin}^y = g_1 \frac{\omega^{3/2}}{\nu^{1/2}} r_p \qquad [17a]$$

$$a_p \nu_{lin}^y \tilde{T}_{lin} + a_p \Omega_\theta \tilde{T}_{rot} + U_\theta \tilde{T}_{transl} = 0 \qquad [17b]$$

From the above force and torque balance, the translation U_θ and rotational Ω_θ velocities of the particle in the angular direction are derived

$$\Omega_\theta = -\frac{U_\theta}{a_p} \frac{\tilde{T}_{transl}}{\tilde{T}_{rot}} - \nu_{lin}^y \frac{\tilde{T}_{lin}}{\tilde{T}_{rot}} \qquad [18a]$$

$$U_\theta = \frac{d\theta_p}{dt} = a_p \nu_{lin}^y \frac{\tilde{F}_{lin}\tilde{T}_{rot} - \tilde{F}_{rot}\tilde{T}_{lin}}{\tilde{F}_{rot}\tilde{T}_{transl} - \tilde{F}_{transl}\tilde{T}_{rot}} \qquad [18b]$$

Making the trajectory coordinates (r_p, θ_p, z_p) dimensionless with respect to $H = (z - a_p)/a_p$ the particle radius a_p, the active area of the disk r_D and 2π, and writing $H = (z_p - a_p)/a_p$, $R = r_p/r_D$, and $\Theta = \theta_p/2\pi$, the following set of three nonlinear first order differential equations is obtained

$$\frac{dH}{dt} = -a_p v_{stagn} \frac{\bar{F}_{stagn}}{\bar{F}_{\perp}} - \frac{F_{ext}}{6\pi\mu a_p^2 \bar{F}_{\perp}} \quad [19a]$$

$$\frac{dR}{dt} = \frac{F_{centr}}{6\pi\mu a_p r_D} \frac{\bar{T}_{rot}}{\bar{F}_{rot}\bar{T}_{transl} - \bar{F}_{transl}\bar{T}_{rot}} + \frac{a_p}{r_D} v_{lin}^x \frac{\bar{F}_{lin}\bar{T}_{rot} - \bar{F}_{rot}\bar{T}_{lin}}{\bar{F}_{rot}\bar{T}_{transl} - \bar{F}_{transl}\bar{T}_{rot}} + \frac{a_p^2}{r_D} v_{par}^x \frac{\bar{F}_{par}\bar{T}_{rot} - \bar{F}_{rot}\bar{T}_{par}}{\bar{F}_{rot}\bar{T}_{transl} - \bar{F}_{transl}\bar{T}_{rot}} \quad [19b]$$

$$\frac{d\Theta}{dt} = \frac{a_p}{2\pi} v_{lin}^y \frac{\bar{F}_{lin}\bar{T}_{rot} - \bar{F}_{rot}\bar{T}_{lin}}{\bar{F}_{rot}\bar{T}_{transl} - \bar{F}_{transl}\bar{T}_{rot}} \quad [19c]$$

This set of equations constitutes the trajectory equations for a particle near a RDE. The particle trajectories are readily calculated by numerical integration of these equations, given the various dimensionless drag forces. The expressions for the drag forces were derived from the work of Brenner (9), Dean and O'Neill (11), O'Neill (10), and Goren and O'Neill (8) together with the limiting values of $\bar{F}_{stagn}$, $\bar{F}_{lin}$, and $\bar{F}_{par}$ from the work of Goren (12), O'Neill (13) and Goren and O'Neill (8) for a spherical particle tangent to a plane

$$\bar{F}_{lin} = 1.701, \bar{F}_{par} = 1.943, \text{ and } \bar{F}_{stagn} = 3.230 \quad [20]$$

When the sphere almost touches the disk, the solutions of the asymptotic lubrication theory are used (14) instead of these exact solutions, which converge poorly for small dimensionless gaps. The only force not yet specified is F_{ext}, for which an appropriate expression will be derived in the next section. The trajectory equations describe the motion of particles with $a_p > 1$ μm. Smaller particles are subjected to random forces, originating from the thermal agitation.

Deriving the External Force Acting on a Particle

The trajectory of a particle depends on the sum of all forces acting upon it. Therefore, the external force needs to be described as accurately as possible, respectively, at large and short distances from the electrode. Close to an electrode, a particle experiences various forces *e.g.* the London dispersive force and the double layer force, while other forces operate in the bulk of the solution.

Long range forces.—Besides the hydrodynamic forces, the only forces that act in the bulk of the suspension are the gravity, the buoyancy, and the electrophoretic force. The net gravity ($\mathbf{F}_g$) and buoyancy force ($\mathbf{F}_b$) are given by

$$\mathbf{F}_g - \mathbf{F}_b = (m_p - m_f)g\mathbf{i}_z = \frac{4}{3}\pi a_p^3(\rho_p - \rho_f)g\mathbf{i}_z \quad [21]$$

The direction of gravity is assumed to be parallel to the axis of the disk, such that the net force is normal to the disk. The electrophoretic force ($\mathbf{F}_{electro}$) has to be considered since an electrical field is present in the solution during electrolytic codeposition. This electrical field acts on the ions present in the double layer around a particle and sets up a tangential fluid flow proportional to the local electrical field. For particles whose double layer is thin compared to the particle diameter, the resulting electrophoretic force in an unbounded fluid is

$$\mathbf{F}_{electro} = \frac{3}{2}\epsilon\zeta_p a_p \mathbf{E} \quad [22]$$

with ϵ the fluid permittivity, ζ_p the zeta potential of the particle surface, and $\mathbf{E}$ the electrical field at the center of the particle. This equation was derived by Smoluchowski and applies to particles of any shape, but it neglects the presence of bounding walls. In codeposition, a particle moves in the neighborhood of a (rotating) electrode. The presence of the electrode affects the electrophoretic force in two ways; the electrode modifies the electrical field, thereby slowing down the particle and the electrophoretic flow is enhanced by the wall, increasing the electrophoretic force.

The electrophoretic force on an insulating particle near a conducting plane was solved by Morrison and Stukel (15) using bispherical coordinates and by Keh and Anderson (16) using the method of reflections, valid for larger particle-to-electrode separations. Although Morrison and Stukel's theoretical analysis is legitimate, their numerical computations are incorrect. Using an analogous method (17), the correct closed form expression for the electrophoretic force is found to be

$$\mathbf{F}_{electro} = 8\pi a_p \epsilon\zeta_p \mathbf{E}_{\perp} \sum_{n=1}^{\infty} \frac{b_n}{2n+3} \quad [23]$$

with the following expression for the b_n coefficients

$$b_n = n(n+1)\frac{\left(n+\frac{3}{2}\right)\sinh\xi_0 \sinh\left(n+\frac{1}{2}\right)\xi_0}{\sinh^2\left(n+\frac{1}{2}\right)\xi_0 - \left(n+\frac{1}{2}\right)^2\sinh^2\xi_0} \left\{ \frac{n-1}{2\cosh\left(n-\frac{1}{2}\right)\xi_0} - \frac{\left(n+\frac{1}{2}\right)\cosh\xi_0}{\cosh\left(n+\frac{1}{2}\right)\xi_0} + \frac{n+2}{2\cosh\left(n+\frac{3}{2}\right)\xi_0} \right\} \quad [24]$$

where ξ_0 is equal to $\ln\{(H+1) + \sqrt{(H+1)^2 - 1}\}$. The net effect is a monotonic increase of the electrophoretic force as the particle-to-surface separation decreases. More particularly, for small gap widths, the electrophoretic force is increased severalfold, approaching a limiting value of 5.138 times the bulk electrophoretic velocity when the particle is in contact with the electrode. Equation [24] is reliable as long as the Debye screening length is much smaller than a_p and the gap width between particle and wall, assumptions which are generally valid in concentrated plating baths.

Dispersion forces.—The dispersion force arises between the instantaneous dipoles that compose the particle and the dipoles induced in neighboring atoms of the electrode and vice versa. There are two essential approaches to the solution of the van der Waals force. Historically, the force between two bodies is simply the incremental pairwise sum of all interactions between all molecules or atoms residing in the two bodies. In that theory, the London-van der Waals force ($\mathbf{F}_{LvdW}$) for a sphere of radius a_p, separated from the electrode across a gap of width h, is given in terms of a Hamaker constant A_{132}

$$\mathbf{F}_{LvdW} = -\frac{2}{3}\frac{A_{132}a_p}{h^2(h+2a_p)^2}\mathbf{i}_z \quad [25]$$

A number of arguments have been raised against this formula; the Hamaker constant A_{132} is only constant with respect to h in the limit of very small or very large separations, the assumption that the force is simply the pairwise summation of all interactions was found to be wrong, and at large separations, compared to the characteristic absorption wavelength of the media, the van der Waals interaction diminishes due to the finite time required by the charge fluctuations to bridge the gap. Most studies involving colloidal interactions have treated the Hamaker con-

stant as an adjustable parameter that was varied in order to best fit theoretical and experimental findings (18). Such gross approximation was avoided here, using the theory put forward by Dzyaloshinskii, Lifshitz, and Pitaevskii (DLP) (19). This continuum theory derives the van der Waals force acting between macroscopic bodies from the dielectrical spectra $\epsilon(\omega)$ of the individual materials. Due to the slow convergence of the quantum mechanical solutions, an alternative strategy was adopted. The retarded van der Waals force is written as the product of the exact Hamaker coefficient for two half-spaces and the Hamaker geometrical factor for the interaction of a sphere with a half space (20). Since none of the involved materials have an appreciable magnetic susceptibility, the DLP formula for the Hamaker coefficient, A_{132}, between two half spaces of material 1 and 2 across a planar slab of material 3 is

$$A_{132} = -\frac{3}{2} kT \sum_{n=0}^{\infty'} \int_{r_n}^{\infty} x \ln(1 - \Delta_{13}\Delta_{23} \exp(-x)) (1 - \bar{\Delta}_{13}\bar{\Delta}_{23} \exp(-x))\, dx \quad [26a]$$

$$\Delta_{j3} = \frac{\epsilon_j s_3 - \epsilon_3 s_j}{\epsilon_j s_3 + \epsilon_3 s_j} \quad \text{and} \quad \bar{\Delta}_{j3} = \frac{s_3 - s_j}{s_3 + s_j} \quad [26b]$$

$$s_j^2 = x^2 + \left(\frac{2\xi_n h}{c}\right)^2 (\epsilon_j - \epsilon_3) \quad [26c]$$

$$r_n = \frac{2h\xi_n\sqrt{\epsilon_3}}{c} \quad n = 0, 1, 2, \ldots \quad [26d]$$

$$\xi_n = \frac{2\pi n kT}{\hbar} \quad n = 0, 1, 2, \ldots \quad [26e]$$

$$\epsilon_j = \epsilon_j(i\xi_n) \quad n = 0, 1, 2, \ldots \quad [26f]$$

The quantities T, k, $2\pi\hbar$, and c are absolute temperature, Boltzmann's constant, Planck's constant, and the velocity of light in vacuum, respectively. The prime on the summation sign indicates that the $n = 0$ term be multiplied by 1/2 and ϵ_j are the dielectrical susceptibilities of the respective materials. The DLP formula needs modification, since in codeposition the intervening media is a strong electrolyte (21). The free ions in the intervening medium screen the static dipole term ($n = 0$) at separations of the order of the Debye length κ_m^{-1}. The integration variable x in Eq. [26] is then replaced in the zeroth frequency term by

$$\sqrt{x^2 + (2\kappa_m h)^2} \quad [27]$$

and the Debye length κ_m^{-1} is given by

$$\kappa_m^{-1} = \left(\frac{\epsilon_m(0) kT}{4\pi e^2 \Sigma_i n_i z_i^2}\right)^{1/2} \quad [28]$$

where n_i and z_i are the number concentrations and charges of each ionic species i, e is the electronic charge, and ϵ is the dielectric permittivity of the electrolyte. The dielectrical functions of the various materials as a function of the frequency ω of the electric field were derived from available optical data using Parsegian's and Weiss method (22) for the representation of $\epsilon(\omega)$

$$\epsilon(\omega) = 1 + \sum_i \frac{f_i - i\omega h_i}{\omega_i^2 + g_i(-i\omega) + (-i\omega)^2} \quad [29]$$

where the coefficients f_i, ω_i, g_i, and h_i are the oscillator strengths, resonant frequencies, bandwidth terms, and fitting coefficients, respectively.

Double layer forces.—Double layer interactions between a particle and the electrode occur due to the overlap of the double layers of particle and wall. The double layers are greatly compressed in electroplating baths because of the high electrolyte concentration. This means that double layer forces are not effective in bringing particles to the electrode. However, their role in the adhesion force cannot be ruled out. The electrostatic force is determined by the distribution of space charge and electrical potential between the particle and the electrode, as described (23) by the nonlinear Poisson-Boltzmann (PB) equation

$$\nabla^2\psi = \frac{8\pi cez}{\epsilon} \sinh \frac{ze\psi}{kT} \quad [30]$$

and by the electrostatic boundary conditions prevailing at their surface. The approximate expression for the double layer force between a sphere and a plate developed by Hogg, Healy, and Fuerstenau (HHF) was used (23, 24). The electrostatic force of the HHF approximation for a plate and particle with constant potential is

$$F_{HHF}^{\psi-\psi}(h) = -\frac{\epsilon\kappa a_p}{2[1 - \exp(-2\kappa h)]} \{2\psi_1\psi_2 \exp(-\kappa h) - (\psi_1^2 + \psi_2^2) \exp(-2\kappa h)\}\mathbf{i}_z \quad [31]$$

and the corresponding expression for a particle with constant surface charge approaching a plane of constant potential is given by

$$F_{HHF}^{\psi-\sigma}(h) = \frac{\epsilon\kappa a_p}{2}\left\{\psi_1\psi_2 \frac{\cosh(\kappa h)}{1 + \sinh^2(\kappa h)} - (\psi_1^2 - \psi_2^2) \frac{\exp(-2\kappa h)}{1 + \exp(-2\kappa h)}\right\}\mathbf{i}_z \quad [32]$$

where ϵ is the dielectrical constant of the electrolyte, ψ_1 and ψ_2 are the surface potentials, h is the separation between the two surfaces, and κ is the inverse Debye length. Due to the Derjaguin approximation, the HHF formulas are limited to low surface potentials (<25 mV) for $a_p\kappa$ values > 10 (*i.e.*, relative high ionic strength and/or relative large particles) and at reasonably large separations. The above equations are appealing because of their simplicity and give reasonable values of the 'exact' double layer force. One of the sources of error is the behavior of the surface potential as the surfaces approach each other. As the characteristic time for the capture of a non-Brownian particle by the rotating disk electrode is short (as compared to the approach under Brownian diffusion for much smaller particles) it seems unlikely that the exchange current density, *i.e.*, the transport of charge across the double layer of the particle, occurs rapidly enough, allowing the particles to keep their surface potential constant. On the contrary, the exchange current density on a metal electrode is significantly larger, so that it can be assumed that the surface potential of the electrode remains constant. Therefore, when calculating the volume flux of particles colliding with the electrode, the double layer interaction with constant surface charge was taken, while in the calculation of the adhesion force, a constant surface potential was assumed.

Concentration and potential field.—The electric field $\mathbf{E}_\perp$ and the Debye length κ_m^{-1} are required to calculate the electrophoretic force, the double layer force, and the Hamaker coefficient. The two dimensional concentration and electric field distributions near the RDE were obtained by the orthogonal collocation technique of Caban and Chapman (25). In that method, the current distribution $i(r)$ on the disk is approximated as a sum of orthogonal polynomials of the form

$$i(r) = \sum_{n=0}^{N-1} A_n P_{2n}(r) \quad [33]$$

where P_{2n} are Legendre polynomials of order $2n$, N is the number of radial collocation points, and A_n are the coeffi-

cients of the current series. From this current distribution, the potential anywhere in the solution can be found

$$\phi = \sum_{n=0}^{N-1} B_n P_{2n}(\eta) \frac{Q_{2n}(i\xi)}{Q_{2n}(0)} \quad [34]$$

with Q_{2n} the Legendre polynomials of the second kind and imaginary argument (26). η and ξ are rotational elliptic coordinates related to the cylindrical coordinate r, z through

$$z = r_D \xi \eta \quad [35a]$$

$$r = r_D \sqrt{(1 + \xi^2)(1 - \eta^2)} \quad [35b]$$

The surface concentration of the Cu^{2+} ions on the disk is given by

$$c(r, 0) = c_\infty + \frac{nFD}{\Gamma(2/3)\hat{t}} \left(\frac{3D_{Cu}}{\nu r_D}\right)^{1/3} \left(\frac{\nu}{\omega}\right)^{1/2} \int_0^r \frac{i(x)x}{[r^3 - x^3]^{2/3}} dx \quad [36]$$

in which $\hat{t}$ and D_{Cu} are the transport number and the diffusion coefficient of the copper ions, n is the number of electrons exchanged in the reduction of one ion, Γ is the gamma function, and ω is the rotation speed of the electrode (27). The surface concentration is used to obtain the concentration distribution (28) in the solution as

$$c(r, z) = c(r, 0) + [c_\infty - c(r, 0)] \frac{\int_0^x \exp\left(\int_0^z \frac{v_z}{D_{Cu}} dz\right) dz}{\int_0^\infty \exp\left(\int_0^\infty \frac{v_z}{D_{Cu}} dz\right) dz} \quad [37]$$

The concentration profile of the sulfate ions is obtained from the electroneutrality equation

$$c_{SO_4^{2-}}(r, z) = c_{Cu^{2+}}(r, z) + \frac{1}{2} c_{H^+}(r, z) \quad [38]$$

while the concentration of H^+ in the electrolyte is constant below the limiting current density. With the concentration profiles of the various constituents of the plating bath, the Debye length can be obtained from Eq. [28]. The diffusion coefficient of Cu^{2+}-ions in sulfuric acid solutions was obtained by Hinatsu and Foulkes (29)

$$D_{Cu} = [6.33 + 2.69 \log (CuSO_4) + 1.62 \log^2 (CuSO_4) + 0.256 \log^3 (CuSO_4)]10^{-10}, [m^2\ s^{-1}] \quad [39a]$$

and the conductivity (25), viscosity, and density (30) were expressed by the following equations

$$\kappa = 10^2 \times [0.011163 + 0.030798(CuSO_4) + 0.423553(H_2SO_4) - 0.045224(H_2SO_4)^2 - 0.135359(CuSO_4)(H_2SO_4)], [m^{-1}\ \Omega^{-1}] \quad [39b]$$

$$\rho_f = [841 + 124(CuSO_4) + 47(H_2SO_4)] \exp (441/RT), [kg\ m^{-3}] \quad [39c]$$

$$\nu_f = 10^{-11} \times [164 + 48(CuSO_4) + 13(H_2SO_4) + 32(CuSO_4)^2 + 2(CuSO_4)(H_2SO_4) + 3(H_2SO_4)^2] \exp (16{,}280/RT), [m^2\ s^{-1}] \quad [39d]$$

where molar analytical concentrations are used in Eq. [39a] and [39b] and molal concentrations in Eq. [39c] and [39d].

Surface Immobilization of Particles

When a particle comes within a pen width of the electrode, the codeposition behavior as predicted by the trajectory equation becomes erratic. The creeping flow equations predict that an infinite force and torque must be applied to move a particle parallel to the disk, when the particle is in contact with the surface. This implies that all particles contacting the disk become irreversibly captured (perfect sink conditions), since the fluid flow around a RDE produces no hydrodynamic force pulling the particles away from the disk. Such lift forces, necessarily inertial in origin, cannot arise in Stokes flow. However Ambari *et al.* (31), measuring the force experienced by a sphere moving parallel to a plane wall, found a finite force as $h \to 0$. This discrepancy is due to the increasing role played by the roughness of the sphere and plane at very small gap widths or to the fact that the no-slip boundary conditions are no longer valid at small separations (32). Whatever the cause, it is clear that dimensionless gap widths H smaller than about 10^{-4} are beyond the purview of the trajectory analysis. Moreover, the trajectory equation describes the motion of particles, and as such it is not apt once the particles are fixed on the electrode.

Therefore, the behavior of particles in the immediate vicinity of the disk will be characterized by a reaction term R which is thought to consist of two terms: $R = R_i + R_r$, respectively the particle immobilization term R_i and the removal rate R_r. The advantage of incorporating the reaction term R in the trajectory equation is that the usual applied perfect sink conditions can be avoided and the specific interactions can be accounted for in a more realistic way. In real systems, surface roughness and nonuniform surface charge distributions of particle and electrode produce significant tangential forces which locally act on the particles. This is the reason why particles remain on the electrodes in the presence of hydrodynamic shearing. While the modeling of the specific normal forces has been done with some success, the tangential forces are much less defined. To model these short range tangential forces it is assumed that the tangential force immobilizing a particle is proportional to the normal adhesion force. If the hydrodynamic shearing forces are balanced by interactions in a narrow region of the particle-wall contact, a force balance on the particle can be set up (Fig. 3). Here F_{adh} is the force of adhesion, and F_{stagn} and F_{shear} are the hydrodynamical forces due to the stagnation point flow and the various shear flows. The critical shear force needed to remove a particle is given by

$$F_{shear} = k(F_{adh} + F_{stagn}) \quad [40]$$

where k is the static coefficient of friction. Friction theory is adopted, which assumes that the tangential force localizing the particle is given by the normal force times the friction coefficient k. The shear and stagnation forces are found from the previous analysis. Near the RDE, the total shear force is given by

$$\mathbf{F}_{shear} = 6\pi\mu a_p^2 \{\nu_{lin}^x \tilde{F}_{lin} - \alpha_p \nu_{par}^x \tilde{F}_{par}\} \mathbf{i}_x + 6\pi\mu a_p^2 r_p \nu_{lin}^y \tilde{F}_{lin} \mathbf{i}_y \quad [41]$$

and the stagnation force by Eq. [8]. With this, the adhesion force F_{adh} is found

$$F_{adh} = \frac{6\pi\mu a_p^2}{k} \sqrt{\{\nu_{lin}^x \tilde{F}_{lin} - \alpha_p \nu_{par}^x \tilde{F}_{par}\}^2 + \{\nu_{lin}^y \tilde{F}_{lin}\}^2} - 6\pi\mu a_p^3 \nu_{stagn} \tilde{F}_{stagn} \quad [42]$$

The static coefficient of friction k that relates the critical shearing force needed to remove a particle, to the force of

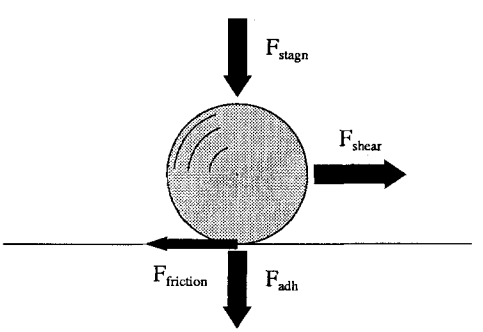

Fig. 3. The various forces acting on a particle near a plane surface.

adhesion, acting normal to the surface, can be invoked from the experimental findings made by Visser (33). Centrifugal measurements of carbon black particles on cellophane showed that the tangential and normal forces required to remove a certain number of adherent particles are equal. This corresponds to a static friction coefficient $k = 1$. The possibility that the friction coefficient will be different in the case of polystyrene particles on electrodeposited copper cannot be ruled out. In steady state, the number of particles immobilized (R_i) on and removed (R_r) from the electrode per unit time equals the flux j_p of particles to the disk, $j_p = R_i + R_r$. The probability p_i that a particle, in contact with the electrode, remains on the electrode, depends on the local ratio of the forces immobilizing the particle $k(F_{adh} + F_{stagn})$ to the removal force F_{shear}. Since it is assumed that a particle is removed once the shear force becomes greater than the total normal force, the probability p_i is given by the following integral

$$p_i = \frac{\int_{F_{shear}}^{\infty} (f_{adh}(F) + F_{stagn})dF}{\int_0^{\infty} (f_{adh}(F) + F_{stagn})\,dF} \qquad [43]$$

where $f_{adh}(F)$ is the differential distribution of the adhesion force of a particle on the electrode. The denominator normalizes the probability, while the numerator is the probability that the normal force is greater than the shear force. The distribution $f_{adh}(F)$ arises because the adhesion force between a particle and the electrode depends on the local physical and geometrical imperfections and on the size of the particle. The probability p_i is a function of position, time, the size of the particle, the current density, and the fluid flow velocities, and it should be looked upon as the instantaneous probability that a particle remains on the electrode. Since particles passing nearby exert random forces on particles residing on the surface, an immobilized particle may be removed at a later instant. The first instant is, however, the most critical since in later instances metal grows around the particle, leading to a lowering of the tangential removal force and a concomitant increase in the normal adhesion force. The probability that a particle in contact with the electrode will codeposit is given by the time average $<p_i>$ of the instantaneous probability p_i. Using Eq. [43] the immobilization rate R_i is given by $j_p p_i$ and $R_r = j_p(1 - p_i)$.

Experimental

To test the trajectory and force descriptions on electrolytic codeposition, experiments were conducted in which polydisperse spherical polystyrene particles were codeposited with copper on a RDE. Polystyrene was used because lattices of polystyrene are easily prepared and used in paints and as a research tool. Also, the spectral properties of polystyrene as required for the van der Waals force computation are known with great precision (22). Complications result from the nonuniform current distribution over the RDE (25) and the geometrical imperfections of the electrolytic polycrystalline deposit, yielding line, and point intersections. With the RDE (ø5 cm) used, a laminar fluid flow of well controlled intensity is set up to Reynolds numbers of 10^5-10^6, implying rotation speeds well in excess of 10,000 rpm (34). The effect of rotation speed, radial position, and current density on the amount of particles codeposited was investigated. The codeposition experiments were thus conducted under conditions sufficiently close to those used in the trajectory calculation. The results will therefore provide necessary criteria to put the theory to the test. They will also provide significant insight and information on the electrolytic codeposition process and are therefore essential to the improvement and refinement of the theoretical analysis.

Experimental procedures.—All experiments involving the codeposition of polystyrene particles were performed in a double walled, 1 liter Pyrex unbaffled cell, thermostated at 21°C, with an OFHC copper counterelectrode mounted flush in the bottom. The experiments were done with a copper plating bath containing 0.8 mol/l $CuSO_4$ $5H_2O$ (analytical grade or better) and 0.2 mol/l H_2SO_4. Deposition was carried out on interchangeable degreased brass electrodes, with an active radius of 1.5 cm mounted in a PTFE holder. Copper was selected since the E° of the Cu(II)/Cu exchange is positive to the H^+/H_2 system. Moreover, by using a copper sulfate electrolyte of low pH, complications due to a hydroxide ion adsorption at the electrode or the presence of an oxide or hydroxide film are avoided. The concentration of polystyrene particles in the bath was measured gravimetrically. The polystyrene particles used were prepared (2) by adding a 10% (w/v) polystyrene solution in 100 ml CH_2Cl_2 (methylenedichloride, b. p. 40°C) to a solution of water containing 1% (w/v) gelatin as protective colloid, under vigorous stirring with a double bladed stirrer. The particle size distribution, measured with a Coulter Electronics Inc. LS100 laser diffraction instrument is shown in Fig. 4. The size distribution $f(a_p)$ was represented by a modified beta function

$$f(a_p) = \frac{x^{mn}(1 - x)^m}{\int_0^1 x^{mn}(1 - x)^m\,dx} \qquad [44]$$

where x is the normalized particle radius defined by

$$x = \frac{a_p - a_{p_{min}}}{a_{p_{max}} - a_{p_{min}}} \qquad [45]$$

A beta function was favored over a Gaussian distribution in view of the finite size range and the shape of the size distribution (35). The surface coverage of codeposited particles was obtained by quantitative image analysis (QIA) techniques of scanning electron micrographs. The volume percentage of codeposited particles is proportional to the surface concentration with the proportionality constant equal to 0.80. The proportionality constant is independent of the diameter distribution function of the codeposited particles, as long as the roughness of the copper deposit is much smaller than the diameter of the smallest particles present. The data sets were smoothed and differentiated by a convolution, least squares Savitzky-Golay method (36).

Zeta potential measurements.—The zeta potential of the polystyrene particles produced at higher rotation speeds (ultraturrax, 20,000 rpm), was determined in the plating bath using a Zetasizer IIc, Malvern Instruments Limited. A positive ζ potential of 13.5 ± 0.5 mV was measured. Although polystyrene particles can be regarded as model particles, anomalous behavior may result from the surface roughness of the particles (37). Dangling bonds and polymer hairs protruding from the particle surface could lead

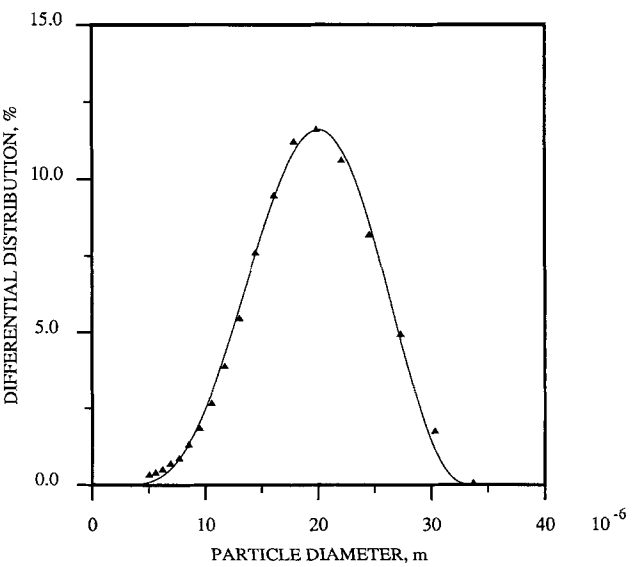

Fig. 4. Particle diameter distribution.

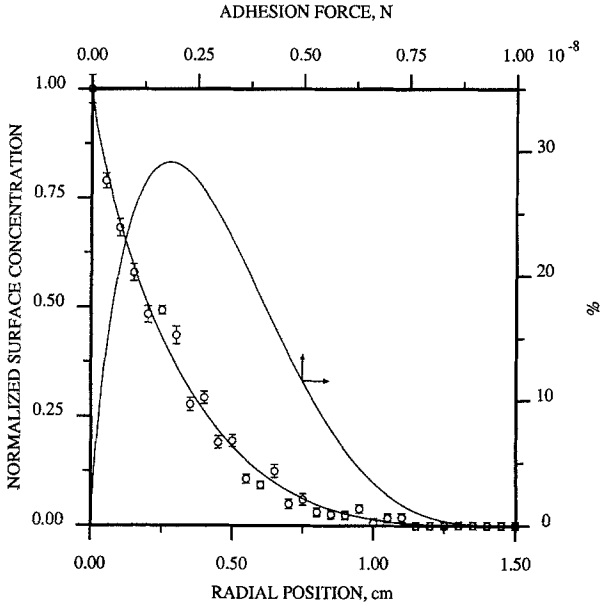

Fig. 5. Normalized surface coverage of polystyrene particles codeposited with copper on a RDE (200 rpm) at 2 A dm^{-2}. The adhesion force distribution for this particular case is also shown.

to an increase in the codeposition efficiency. By heating the polystyrene particles above their glass transition temperature (100°C, for 6h), any dangling bonds will collapse onto the surface of the particles, resulting in a shift of the shear plane and thus of the measured ζ potential. However, the ζ potential of the heat-treated particles was still 14.4 ± 1.2 mV, so that it can be concluded that the polystyrene particles do not possess protruding bonds. In order to establish the sign of the charge of the copper electrode near rest potential, the ζ potential of very fine copper powder ($\approx$ 1 μm) prepared by the polyol method (38), was measured. A positive zeta potential of 6.4 mV was found. This was anticipated because a metal, in contact with its own ions, has an appreciable exchange current, leading to a local surplus of positive charge in the double layer. As the copper powder slowly dissolves in the acid plating bath, the surface properties of the oxide free copper powder are probably close to those of a copper electrode immersed in the same electrolyte. It can thus be concluded that, near rest potential, the surface of the copper electrode in contact with the plating bath is positively charged.

Experimental codeposition results.—The experimentally measured surface fraction of polystyrene particles codeposited with copper at a current density of 2 A dm^{-2} and rotation speed of 300 rpm is shown in Fig. 5. The surface fraction $\theta(r)$ is normalized with respect to the surface coverage $\theta(0)$ in the center of the disk

$$\tilde{\theta}(r) = \frac{\theta(r)}{\theta(0)} \qquad [46]$$

As can be seen, the surface concentration of codeposited particles varies markedly with radial position. From measurements done at various rotation speeds, the concentration has been found to fall off more rapidly as the rotation speed of the electrode increases. According to the trajectory equations (Eq. [19a], [19b], and [19c], the flux of particles should be statistically independent of the radial position. Therefore, the measured dependence of surface coverage of codeposited particles is not caused by the incident rate of particles colliding with the disk, but may be related to the radial dependence of the immobilization reaction R_i. As the shearing force increases with an increase in the radial position of the disk, R_i decreases, because particles with higher adhesion forces leave the surface, depending upon the relative magnitude of the hydrodynamic shearing force and adhesion (contact) forces. The particle-cathode adhesion force can be inferred from the variation of the removal rate with radial position along the disk. The shearing force that removes 50% of the particles is taken as the adhesion force of a particle with a diameter equal to the average diameter using Eq. [42], while the drop in codeposition as a function of the applied shear stress can be used to obtain the distribution of the adhesion forces $f_{adh}(F)$ of all particles present during codeposition. $f_{adh}(F)$ is represented by the modified beta function used before (Eq. [44])

$$f_{adh}(F) = \frac{F^{a-1}(1-F)^{b-1}}{\int_0^1 F^{a-1}(1-F)^{b-1}\,dF} \qquad [47]$$

where F is the adhesion force normalized against the maximum adhesion force $F_{adh_{max}}$

$$F = \frac{F_{adh}}{F_{adh_{max}}} \qquad [48]$$

The parameters a and b of the distribution were found by fitting the cumulative distribution, which is defined as the integral of the differential distribution

$$\frac{\int_0^F x^{a-1}(1-x)^{b-1}dx}{\int_0^\infty x^{a-1}(1-x)^{b-1}dx} \qquad [49]$$

to the measured concentration profile of codeposited latex particles. Both distributions are shown in Fig. 5.

The surface coverage of the electrode at the center of the disk *vs.* the concentration of particles in the bath is shown in Fig. 6. The surface coverage of the electrode at the center of the disk was extrapolated from surface coverage determinations done along a radius of 3 mm from the center. This was done to improve the statistical significance, especially at low surface coverage. The data from Fig. 6 can be used to compare the theoretical codeposition rate with the experimental one. The theoretical surface coverage at a certain current density is calculated as

$$\theta = \frac{\left(1-\frac{\theta}{\theta_m}\right)j_p}{\left(1-\frac{\theta}{\theta_m}\right)j_p + j_m} \qquad [50]$$

where j_p and j_m are the volume of particles colliding with the electrode and the volume of metal that codeposits per

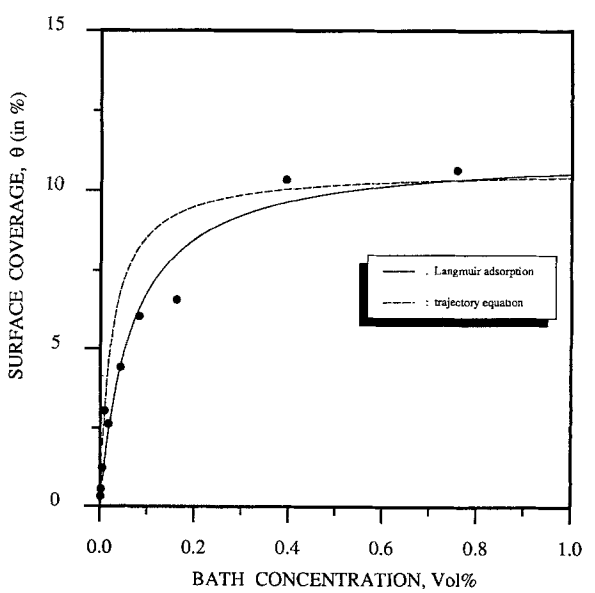

Fig. 6. Measured surface coverage at the center of the rotating electrode *vs.* the particle concentration in the bath.

Table II. Experimental and theoretical codeposition volume percentages for the system polystyrene particles/copper.

Bath concentration (Vol. %)	Vol % of codeposited particles			
	Experimental (QIA)	No shielding $\theta_m = 0.547$	With shielding $\theta_m = 0.133$	Langmuir adsorption $\theta = \frac{k}{1 + kc}$
0.0007	0.40	0.48	0.47	0.15
0.0014	0.70	0.94	0.90	0.30
0.0035	1.56	2.24	2.01	0.72
0.0071	3.81	4.17	3.44	1.35
0.014	3.29	7.34	5.37	2.40
0.034	5.53	13.70	8.19	4.47
0.065	7.55	19.59	9.98	6.28
0.129	8.20	26.01	11.36	8.01
0.315	12.93	33.37	12.44	9.63
0.606	13.30	37.32	12.85	10.33

unit time, respectively, and θ_m is the maximum surface coverage that can occur under the given conditions of particle size distribution $f(a_p)$ and current density i. Codeposited particles change the geometry of the disk and thus the conditions for depositing subsequent particles. If it is assumed that only particles landing on an unoccupied area of the disk are amenable for codeposition, the former equation is motivated by the fact that $(1 - \theta/\theta_m)$ is the probability that a particle hits the surface in such an area.

From the trajectory equations, the volume flux of particles colliding with the rotating disk j_p is calculated as the flux of particles within the limiting particle trajectory. The limiting particle trajectory is defined as the particle trajectory that divides incoming particle trajectories with terminal contact from those which pass by. The limiting particle trajectory is obtained by integrating the trajectory equations of a particle that just manages to be captured by the disk, backwards in time, until its motion coincides with the undisturbed streamlines. In this work the limiting trajectory was taken at a dimensionless distance of $H = 10$. The volume flux j_p of particles colliding with the disk per unit time is given by

$$j_p = c \int_{a_{pmin}}^{a_{pmax}} \frac{4}{3} \pi a_p^3 V_z \pi r_{limit}^2(a_p) f(a_p) da_p \qquad [51]$$

where V_z is the fluid flow velocity at the axial distance where the particle trajectories coincide with the fluid motion, r_{limit} is the radial position of the limiting trajectory, and c is the volume concentration of particles in the bath. The volume rate of metal deposition is found from

$$j_m = \frac{iA_{Cu}}{nF\rho_{Cu}} \qquad [52]$$

with A_{Cu} and ρ_{Cu} the molecular weight and density of copper, respectively. Table II compares the measured surface concentration with the theoretically calculated surface coverage according to Eq. [50]. Three different cases were calculated. In the first, shielding was assumed to be absent and the jamming limit of 0.547 for noninteracting monosized disks, randomly placed on a surface, was taken as the maximum surface coverage. The maximum surface coverage in our case is probably larger, since we are dealing with polydisperse particles. In the second, the shielding parameter was varied in order to fit at best the experimental values, while the third is the Langmuir adsorption isotherm. The close resemblance between Eq. [50] and the Langmuir adsorption isotherm explains the use of the latter in the electrolytic codeposition model of Guglielmi (3). The correspondence between the experimental and theoretical values is satisfactory knowing that any calculation of the codeposition rate is necessarily approximate since the collision rate depends on the flocculation of the particles in the bath and on the behavior of the particles or flocs when they approach and collide with the disk or with previously codeposited particles. The experimental and theoretical values agree well at low surface coverage but diverge at larger surface coverage. This is due, in part, to the shielding by particles which block part of the electrode in their immediate vicinity and the disruptive hydrodynamical and specific forces that are exerted on deposited particles by particles flowing in their vicinity (39). It is clear that a deposited particle may be dislodged when these additional forces are comparable to the specific surface forces localizing the particle. These effects are minor for small bath concentrations, but with increasing bath concentrations, the interactions among immobilized particles and those flowing in their vicinity gain importance. At present, no adequate quantitative theory exists that can account for these effects.

Figure 7 gives the integrated (global) surface coverage Θ

$$\Theta = 2\pi \int_0^{r_D} r\theta(r) dr \qquad [53]$$

as a function of applied current density and rotation speed of the RDE. The codeposition is at the highest between 1 and 2 Adm^{-2}. This effect is not predicted by the trajectory equation since the mass transport of particles towards the disk is almost independent of the applied current density. The underlying reason must thus be found in a dependence of the immobilization rate R_i on current density.

Point of zero charge determination.—The maximum codeposition of polystyrene particles in copper occurs in a current density range of 1 to 2 A dm^{-2} corresponding to an overpotential of approximately −100 mV. Also, in the codeposition of γ-Al_2O_3 from acid copper plating baths (40), a maximum in the codeposition curve was reported between 1 and 2 A dm^{-2}. Within the framework of the DLVO

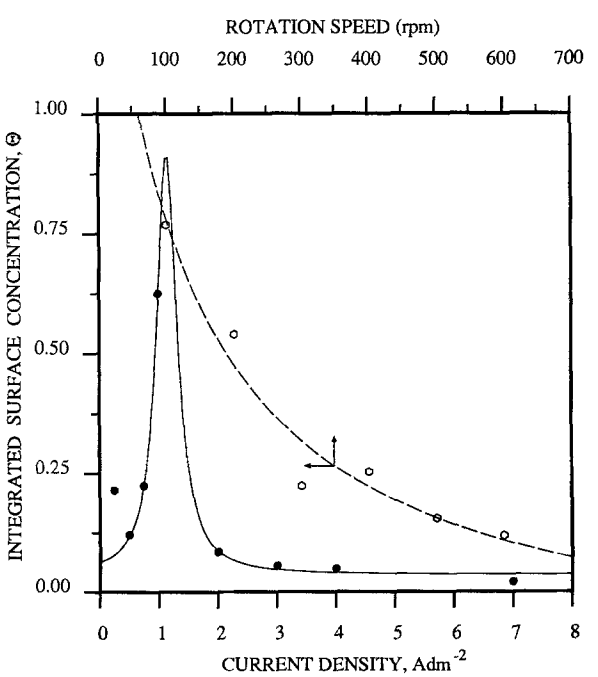

Fig. 7. Integrated normalized surface coverage vs. applied current density and rotation speed.

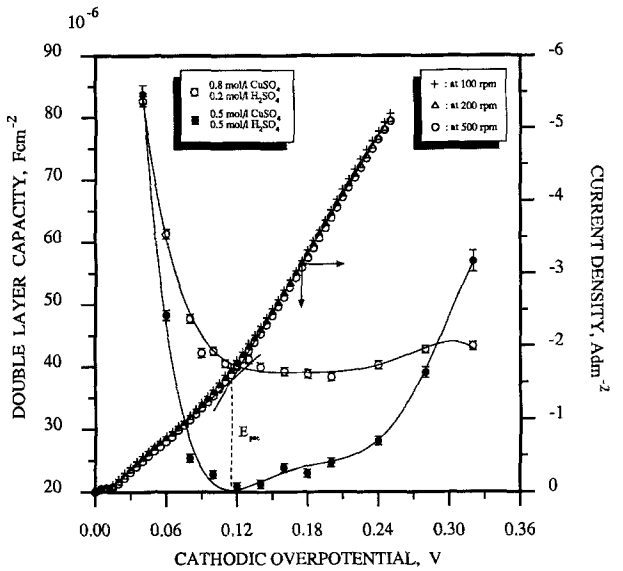

Fig. 8. Overlay graph of the current density and the double layer capacity vs. the applied overpotential.

theory, the electrical double layer force is the only candidate that could account for a shift in the codeposition behavior with current density. Upon polarizing cathodically, the charge of a copper electrode, which is positive near rest potential, changes sign at the potential of zero charge E_{pzc}. Potential step techniques, such as chronocoulometry, have been used to measure the E_{pzc} of solid electrodes, but they fail due to the polarizable nature of the $Cu/CuSO_4$ interface. From theoretical arguments, the position of the E_{pzc} should be discernible on a polarization curve. The existence of a positive charge at the electrode for potentials above the E_{pzc} diminishes the Tafel slope since the positively charged copper ions are less likely to remain in the vicinity of a positively charged electrode. However, at decreasing potentials below E_{pzc}, the rate of copper reduction increases since the ion-transfer is unaffected by double layer effects. It was therefore attempted to obtain the E_{pzc} from polarization measurements. Polarization curves recorded in aerated copper sulfate solutions at three different rotation speeds (100, 200 and 500 rpm) are shown in Fig. 8. On these curves a transition can be seen, where the slope of the current *vs.* applied potential increases markedly. The position of this transition is not affected by the rotation speed. So the change in the reduction rate does not depend on the rate by which copper ions diffuse to the surface but on the electrochemical reduction process itself. The position that marks the beginning of the deviation was found by fitting the following single equation model to the experimental data

$$I = \frac{a + bE}{1 + \exp[f(E - E_t)]} + \frac{c + dE}{1 + \exp[-f(E - E_t)]} \quad [54]$$

where a, b, c, d, and f are empirical constants, and where it was assumed that the potential behavior of the current in both regions is approximately linear. E_t is identified as a transition overpotential, and f is a measure of the sharpness of the transition. From the model, an approximate E_{pzc} value of -115 mV *vs.* $E^{\circ}_{Cu/Cu^{2+}}$ was found.

Russian investigators (41) concluded that in the electrodeposition of copper on [111] copper single crystals, a morphological change at an overpotential of *ca.* -100 mV. Thus, the change in slope could also be due to a change in the growth behavior. However, no difference was seen between the impedance diagrams taken at overpotentials of -60 and -140 mV, making the former explanation improbable. Besides polarization measurements, the E_{pzc} can be determined independently by measuring the double layer capacity as a function of the applied overpotential. At increasing absolute value of the charge on the copper electrode, ions are drawn towards the electrode surface. Accordingly, the average thickness of the double layer must have a maximum and its capacity a minimum at the E_{pzc}. The capacity of the double layer was obtained from impedance measurements. In a certain frequency range, the measured impedance during the electrocrystallization of copper can be modeled with sufficient accuracy by a simple Randles equivalent circuit, where the double layer capacity is in parallel with the charge transfer resistance. The time constant is related to the first step of the reduction: $Cu^{2+} + e^- \rightarrow Cu^+$. However, it has to be noted that this equivalent circuit fails for overpotentials close to the rest potential, where the time constant of other processes in the copper crystallization starts to overlap with the primary one. This is not a serious drawback since the E_{pzc} is sufficiently removed from the rest potential. Double layer capacitances, calculated assuming the simple parallel RC circuit are shown in Fig. 8. Two curves are shown, corresponding, respectively, to the measured capacities of a copper electrode in contact with a copper plating bath containing, respectively, 0.8 mol l^{-1} $CuSO_4$ and 0.2 mol l^{-1} H_2SO_4 and a bath containing 0.5 mol l^{-1} $CuSO_4$-0.5 mol l^{-1} H_2SO_4. The minimum in the double layer capacity is more prominent in the second bath than in the former, which shows no appreciable minimum. Therefore, the minimum of the latter curve was chosen as the point of zero charge and it was assumed that the points of zero charge in both baths are identical. The minimum in the measured double layer capacities occurs at 110 mV *vs.* rest potential, in accordance with literature (42). The coincidence of the E_{pzc} determined by the polarization experiments and the differential capacity measurements forces us to consider the value of the E_{pzc} as sufficiently reliable. It can be concluded that the maximum in the codeposition of polystyrene particles and γ-Al_2O_3 with copper (40) around 1 to 2 Adm^{-2}, are linked to the point of zero charge.

Global Mechanism underlying the Electrolytic Codeposition

As stipulated above, the radial position $r_{50\%}$, where the surface concentration of particles is half that in the center, was used to determine the adhesion force of a particle with a diameter equal to the average diameter

$$F_{adh} = F_{LvdW} + F_{HHF}^{\psi-\psi} + F_g + F_b + F_{electro} \quad [55]$$
$$= F_{shear} - F_{stagn}$$

The separation h where the sum of all normal forces equals the tangential force (for the radial position corresponding to $r_{50\%}$) is the equilibrium distance. The surface potential of the electrode used in the calculation of the double layer force was found from the measured double layer capacities. Therefore the surface charge density of the electrode was obtained by integrating the double layer capacity with potential

$$\sigma_2(E) = \int_{E_{pzc}}^{E} C_{dl}(E)\, dE \quad [56]$$

and the surface potential corresponding to this double layer charge (for noninteracting surfaces) was obtained from the Gouy-Chapman relation

$$\sigma_2 = -\mathrm{sgn}(\psi_2)\left[\frac{\epsilon kT}{2\pi}\sum_i n_{0i}\left\{\exp\left(\frac{z_i e}{kT}\psi_2\right) - 1\right\}\right]^{1/2} \quad [57]$$

where ϵ is the electrical permittivity, n_{0i} and z_i are the concentration and charge of species i in bulk solution, and e is the unit electric charge. The Hamaker coefficient was calculated from Eq. [26]. For water, one microwave relaxation, five infrared and six ultraviolet absorption frequencies were included in the representation of $\epsilon(i\xi_n)$. The complex permittivity of polystyrene was approximated by 4 ultraviolet absorption peaks, while that of copper was fitted by 4 UV absorption peaks and the free electron contribution. The infrared and ultraviolet oscillator strength and absorption pulsations, as well as the static dielectrical constants, were found in literature (22). Computations car-

ried out with 600 terms for n and with piecewise Gaussian quadratures for the integration of the x-variable, give A_{LvdW} (T = 296.14 K) = 4.67 10^{-20} J for polystyrene interacting across water with copper. Due to the strong absorption of electromagnetic waves in water, the effect of electromagnetic retardation sets in early, and cannot be discarded, not even at short distances. If the particle deforms under the adhesion forces, the dispersion force is modified and corrections have to be made to include the additional dispersion force. Although such adhesion force induced deformations between particles and substrate were reported in literature (43), no deformations were seen for the polystyrene particles used in this work, dropped on polished Si-substrates, with the aid of a SEM, operated at an electron beam angle of 80° with the normal on the substrate plane. Since the magnitude of the dispersion forces is about 10 times larger in vacuum than in water, no gross deformation of the polystyrene particles is expected during codeposition, aiding the adhesion of particles. Since the deformation is sufficiently small and the elastic limit of the substrate is not exceeded, a rough estimate of the contact area of the particle can be obtained (44) assuming Hertzian response

$$r_0^3 = \frac{3}{4}\left(\frac{1-\nu^2}{E}\right) a_p F_{adh} \qquad [58]$$

where ν is the Poisson ratio of polystyrene, E is the Young modulus of the substrate, and r_0 is the radius of the deformed contact area. Assuming an adhesion force of 5 × 10^{-9} N, a radius of the deformed area of 0.007 μm is found for a 22 μm diameter particle. The elastic deformation can therefore be disregarded when determining the dispersion force.

In Fig. 9 the adhesion force calculated from the experimentally measured surface (cfr. Eq. [42]) concentrations and the corresponding equilibrium distances are shown as a function of the current density. Figure 9 invalidates the explanation put forward in the previous paragraph, where the maximum in the codeposition was ascribed to the variation of the double layer force with applied current density. If that explanation was right, the measured adhesion force would not show a maximum, corresponding to the point of zero charge, but the adhesion force would increase in magnitude beyond the point of zero charge, because at potentials more negative than E_{pzc} the double layer force is positive and the DLVO theory predicts overall attractive forces. Contrary to this, the measured force drops off on either side of the point of zero charge. Although the exact value of the determined adhesion forces depends on the value of the static friction coefficient k, which was set at 1

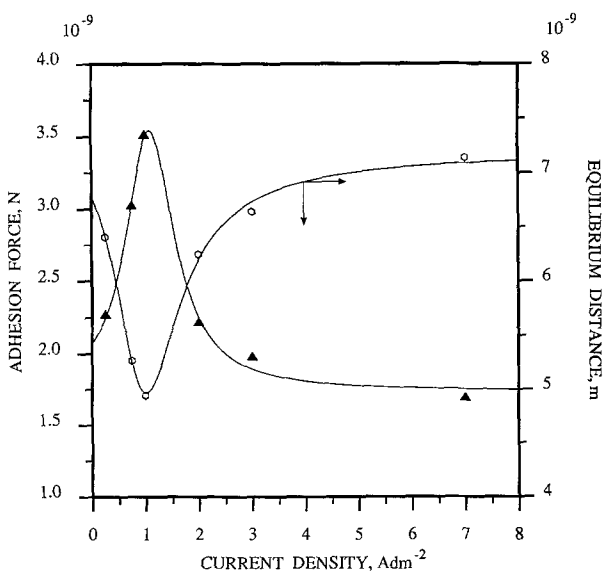

Fig. 9. Calculated adhesion force and corresponding equilibrium distance vs. current density.

in this work, the observed dependence of the adhesion force on current density is not influenced by it. Also, the calculated equilibrium distances in Fig. 9 are too large to be accommodated in any theory which only takes into account the forces mentioned previously.

The relatively large distance of the position of the force minimum implies that the minimum in which the particles reside is a secondary minimum, while the DLVO theory predicts the surfaces to be pulled into primary contact. One should take into consideration the fact that the interactions in electrolytic codeposition occur in very strong electrolytes. From measurements of the interaction force between crossed glass filaments in concentrated KCl solutions (45), a minimum in the dependence of the interaction force on the distance $F(h)$ was found between 6 and 7 nm, corresponding closely to the equilibrium distances obtained in this work. The forces measured between cleaved mica surfaces in a double cantilever beam assembly in dilute solutions (46, 47) have been shown to be well described by the DLVO theory. However, above a certain electrolyte concentration a strong repulsive force is present at short distances. This force does not decay with the Debye length. Moreover, the measured force is oscillatory, with a period that matches the size of the solvent molecules. This force is called the structural or hydration force and is ascribed to the ordering of the solvent near the interfaces usually brought about by the hydration of cations adsorbed onto the surface. This force is of sufficient strength to prevent the van der Waals force from pulling the surfaces into primary minimum contact. From force measurements in electrolyte solutions (48), the force between two parallel surfaces was found to be

$$\mathbf{F}_{hydr} = K \exp(-h/l)\mathbf{i}_z \qquad [59]$$

Theories about the structural force state that the value of the constant K is directly proportional to the degree of ordering of the dipole molecules of the solvent near the interface and the value of the constant l to the corresponding correlation length. The previous formula, valid between parallel plane surfaces has to be modified to describe the particular geometry of a particle interacting with the electrode. A Derjaguin type integration over the surface of the particle leads to

$$\mathbf{F}_{hydr} = Ka_p^2 \int_0^{2\pi} d\theta \int_0^{\pi/2} \sin\psi \cos\psi \exp\left[-\frac{h}{l} - \frac{a_p}{l} + \frac{a_p \cos\psi}{l}\right] d\psi \mathbf{i}_z \qquad [60a]$$

$$= 2\pi a_p^2 K \exp\left[-\frac{h}{l} - \frac{a_p}{l}\right] \left[\frac{l \exp\left(\frac{a_p}{l}\right)}{a_p}\left[l - \frac{l}{a_p}\right] + \left(\frac{l}{a_p}\right)^2\right] \mathbf{i}_z \qquad [60b]$$

where h is the distance of closest approach between the surfaces. As the correlation length l is of the order of 0.1 to at most a few nanometer, $l/a_p << 1$, the force is well approximated by the following formula

$$\mathbf{F}_{hydr} = 2\pi a_p K l \exp(-h/l)\mathbf{i}_z \qquad [61]$$

From the determined equilibrium distances the preexponential factor K of the hydration force was found to be 4.5 10^6 [Nm^{-2}], assuming a decay length l of 1 nm. This is in agreement with the hydration force constants found in literature (48). In general it can be said that the hydration force is caused by a change in the structure of the solvent under the influence of the substrate force field. As such, the variation of the adhesion force with the current density as shown in Fig. 9 can be understood. At the point of zero charge, the electric field at the electrode is minimal and so is the orientational ordering of the water dipoles. Left or

right from the point of zero charge the electric field near the electrode increases in magnitude and the water dipoles line up, either flipped up or down according to the sign of the electric field. This increases the ordering of the solvent and leads to a larger value of K. Thus the maximum in the codeposition coincides with a minimum in the structural force. This might also explain why highly hydrophilic materials such as quartz and most oxides have a small tendency to codeposit due to the hydrolyzable nature of their surface. On the other hand, hydrophobic surfaces, such as some plastics (49), graphite (50), Si_3N_4 (51), and other nitrides and carbides, codeposit readily, under the prerequisite that the material can be kept in suspension during electrolysis. Since the value of K is positive for lyophilic systems and negative for hydrophobic surfaces, indicating attraction, this might also explain the comparatively large codeposition of PTFE and other polyfluorcarbon compounds (52), notwithstanding their lower dispersion force. The codeposition promoting character of monovalent cations like thallium, rubidium, and cesium (53) might be attributed to the fact that these ions become adsorbed to the surface of the particle and, due to their weakly bound hydration sheets, lower the solvation force around the particle. Moreover, the effect of various surfactants that increases codeposition at low concentrations but suppresses codeposition when present in high concentrations (54) might in part be understood as due to the hydration force. At concentrations lower than the critical monolayer coverage, most surfactants render the surfaces hydrophobic (55). This occurs since the surfactant molecules are adsorbed with their polar head towards the particle and their hydrophobic tail pointed towards the solution. Increasing the surfactant concentrations beyond the critical monolayer coverage reverses this effect. Although it is tempting to ascribe the experimental results to the presence of the hydration force, the proof offered so far is indirect and tenacious. Therefore, attempts should be set up to directly measure the adhesion force between a particle and an electrode immersed in an electrolyte.

Conclusion

A particle remains on an electrode if the ratio of the normal to tangential forces acting on the particle when it first hits the surface is favorable. If this condition is satisfied, a particle brought in contact with the electrode has enough foothold to remain on the electrode and be engulfed by the growing metal. In the center of a RDE, tangential forces are absent and the rate of codeposition is controlled solely by the mass transfer of particles towards the rotating electrode with due account of surface blockage and hydrodynamic shielding.

The analysis and calculations presented in this paper indicate that the trajectory model is an adequate basis for studying the electrolytic codeposition of particles on a RDE. The comparison of experimental results with theoretical predictions proves the predominance of the tangential shearing force and, in general, of the fluid flow velocities on the codeposition of particles. The experiments also point out that the lack of useful descriptions of the tangential forces localizing the particles is the most pronounced difficulty in developing useful theories on electrolytic codeposition. This difficulty arises because the models for the normal force all assume a spherical isotropic particle on a flat surface, while tangential forces only emerge if geometrical and physical heterogeneities are taken into account. The need for an adequate representation of the randomness of particles and electrode is thus obvious. It is also essential that the model should be capable of depicting realistically the flow field and include the effect of flowing particles on previously deposited particles. The rate at which particles are being brought to the electrode is governed almost entirely by the convection instigated by the rotating disk and by the dispersion forces, while the double layer force and electrophoresis can be disregarded. Closer to the electrode, the particle immobilization is dominated by the specific force field generated by the particle-wall interactions. These interactions are of very short range (usually a small fraction of the particle size, distance range of the order of 10 nm), and are described by the classical DLVO theory in combination with an additional repulsive force acting between the surfaces. This force was identified as the hydration force, that comes about in concentrated electrolytes used in electrolytic codeposition. Together with the attractive dispersion force, this gives rise to a secondary minimum in the interactions around 6 nm. The trajectory description used in this work is, however, not limited to the RDE geometry, but can be used for a variety of other geometries. The only prerequisite is an accurate description of the fluid velocities in the immediate vicinity of the cathode. It is also possible to extend the trajectory equations to smaller particles by including a random force that mimics the Brownian agitation, resulting in Langevin type of equations.

Acknowledgments

This work forms part of the Ph.D. thesis of J. Fransaer, who wishes to thank the IWONL for its financial support. This work was also supported by the Belgian Government, within the framework of the Interuniversity Networks for Fundamental Research (Contract IUAP No. 4) and the Commission of the European Community (BRITE/EURAM contract No. CT 91-0402.).

Manuscript submitted May 9, 1991; revised manuscript received October 3, 1991.

Katholieke Universiteit Leuven assisted in meeting the publication costs of this article.

LIST OF SYMBOLS

f_1	0.51023261886728488
g_1	−0.61592201439935397
a_p	particle radius, [m]
f_n, g_n, and h_n	coefficients of the power series in $\sqrt{\omega/v}\,z$
$\tilde{F}_{lin}$, $\tilde{F}_{par}$, $\tilde{F}_{stagn}$, $\tilde{F}_{\perp}$, $\tilde{F}_{rot}$, and $\tilde{F}_{transl}$	hydrodynamic mobility coefficients
$\tilde{T}_{lin}$, $\tilde{T}_{par}$, $\tilde{T}_{rot}$, and $\tilde{T}_{transl}$	hydrodynamic mobility coefficients
$\mathbf{i}_r$, $\mathbf{i}_\theta$, and $\mathbf{i}_z$	unit vectors in cylindrical coordinates
$\mathbf{i}_x$, $\mathbf{i}_y$, and $\mathbf{i}_z$	unit vectors in Carthesian coordinates
v_z, v_r, and v_θ	axial, radial and angular velocity component [ms^{-1}]
r, z	radial and axial position in cylindrical coordinates [m]
E	electrical field, [Vm^{-1}]
p	dynamic pressure, [Nm^{-2}]
F	Faraday constant, 9.648456×10^4 [$C\,mol^{-1}$]
$\mathbf{F}$	force vector, [N]
T	torque vector, [N]
R	gas constant, 8.31441×10^0 [$JK^{-1}\,mol^{-1}$]
k	Boltzmann constant, 1.380662×10^{-23} [JK^{-1}]
c	speed of light in vacuum, 2.99792458×10^8 [ms^{-1}]
N_A	Avogadro constant, 6.022045×10^{23} [mol^{-1}]
h	surface to surface distance between particle and electrode, [m]
$\mathbf{v}$	fluid flow velocity vector, [ms^{-1}]
$\mathbf{u}$	velocity vector of the particle, [ms^{-1}]
e	unit electric charge, $1.6021892 \times 10^{-19}$ [C]
g	acceleration due to gravity, 9.81 [ms^{-2}]

Greek

ω	angular velocity of the disk [rad s^{-1}]
μ	dynamic viscosity [$kg\,m^{-1}s^{-1}$]
ν	absolute viscosity [m^2s^{-1}]
ρ	specific density [$kg\,m^{-3}$]
θ	angular position in cylindrical coordinates [°]
θ	fractional surface coverage, dimensionless

ϵ	$4\pi\epsilon_0\epsilon_r$, $[C^2J^{-1}m^{-1}]$
ϵ_0	permittivity in vacuum, $8.854187818 \times 10^{-12}$ $[C^2J^{-1}m^{-1}]$
ϵ_r	relative dielectrical constant of the fluid, dimensionless
ζ	zeta potential, [V]
κ	reciprocal Debye screening length, $[m^{-1}]$
Ω	angular velocity of a particle, $[s^{-1}]$
∇^2	Laplace operator
∇	gradient operator
ψ	surface potential [V]
$\hbar$	$h/2\pi$, 1.05450×10^{-34} [Js]
Θ	integrated dimensionless surface concentration
σ	surface charge density, $[Cm^{-2}]$

Subscripts

D	disk
o	particle center
p	particle
f	fluid
$\perp$	pertaining to the perpendicular motion
shear	pertaining to the shear flow
stagn	pertaining to the stagnation point flow
lin	pertaining to the linear shear flow
par	pertaining to the parabolic (quadratic) shear flow
rot	pertaining to the rotational motion
transl	pertaining to the translational motion
adh	adhesion

Superscripts

$\sim$	dimensionalized variable
$\hat{}$	disturbance variable
x	x-directional
y	y-directional

REFERENCES

1. J. R. Roos, J. P. Celis, J. Fransaer, and C. Buelens, *Met. Finish.*, **42,** 60 (1990).
2. J. Fransaer, J. P. Celis, and J. R. Roos, *Journal of Metals,* **87,** 107 (1989).
3. N. Gulgielmi, *This Journal,* **119,** 1009 (1972).
4. L. A. Spielman and J. A. Fitzpatrick, *J. Coll. Int. Sci.,* **42,** 607 (1973).
5. L. A. Spielman and P. M. Cukor, *ibid.,* **43,** 51 (1974).
6. R. Rajagopalan and C. Tien, *Can. J. Chem. Eng.,* **55,** 246 (1977).
7. J. Fransaer, J. R. Roos, and J. P. Celis, *Chem. Eng. Sci.,* **46,** 1194 (1991).
8. S. L. Goren and M. E. O'Neill, *ibid.,* **26,** 325 (1971).
9. H. Brenner, *ibid.,* **16,** 242 (1961).
10. M. E. O'Neill, *Mathematika,* **11,** 67 (1964).
11. W. R. Dean and M. E. O'Neill, *ibid.,* **10,** 13 (1963).
12. S. L. Goren, *J. Fluid Mech.,* **41,** 619 (1970).
13. M. E. O'Neill, *Chem. Eng. Sci.,* **23,** 1293 (1968).
14. A. J. Goldman, R. G. Cox, and H. Brenner, *ibid.,* **22,** 637, 653 (1967).
15. F. A. Morrison, Jr. and J. J. Stukel, *J. Coll. Int. Sci.,* **33,** 88 (1970).
16. H. J. Keh and J. L. Anderson, *J. Fluid Mech.,* **153,** 417 (1985).
17. J. Fransaer and J. R. Roos, To be submitted.
18. Y. Suzuki and O. Asai, *This Journal,* **134,** 1905 (1987).
19. I. E. Dzyaloshinskii, E. M. Lifshitz, and L. P. Pitaeviskii, *Adv. Phys.,* **10,** 165 (1961).
20. B. A. Pailthrope and W. B. Russel, *J. Coll. Int. Sci.,* **89,** 563 (1982).
21. V. A. Parsegian, in "Physical chemistry: enriching topics in colloid and surface science," H. Van Olphen and K. J. Mysels, Editors, p. 27 Theorex, La Jolla (1975).
22. V. A. Parsegian and G. H. Weiss, *J. Coll. Int. Sci.,* **81,** 285 (1981).
23. R. Hogg, T. W. Healy, and D. W. Fuerstenau, *Trans. Faraday Soc.,* **62,** 1638 (1966).
24. G. Kar, S. Chander, and T. S. Mika, *J. Coll. Int. Sci.,* **44,** 347 (1973).
25. R. Caban and T. W. Chapman, *This Journal,* **124,** 1371 (1977).
26. J. Newman, *ibid.,* **112,** 501 (1966).
27. J. Newman, *ibid.,* **113,** 1235 (1966).
28. V. G. Levich, "Physicochemical Hydrodynamics," Prentice-Hall, Inc., Englewood Cliffs, N.J. (1962).
29. J. T. Hinatsu and F. R. Foulkes, *This Journal,* **136,** 125 (1989).
30. J. Hotlos and M. Jaskla, *Hydrometallurgy,* **21,** 1 (1988).
31. A. Ambari, B. Gauthier Manuel, and E. Guyon, *J. Phys., Lett.,* **44,** L143 (1983).
32. L. M. Hocking, *J. Eng. Math.,* **7,** 207 (1973).
33. J. Visser, *J. Coll. Int. Sci.,* **34,** 26 (1970).
34. P. Mishra and P. C. Singh, *Chem. Eng. Sci.,* **33,** 1449 (1978).
35. L. M. Popplewell, O. Campanella, and M. Peleg, *Powder Technol.,* **54,** 157 (1988).
36. P. A. Gorry, *Anal. Chem.,* **62,** 570 (1990).
37. R. S. Chow and K. Takamura, *J. Coll. Int. Sci.,* **125,** 226 (1988).
38. F. Fievet, J. P. Lagier, and M. Figlarz, *MRS Bulletin,* **14,** 29 (1989).
39. T. Dabros, *Coll. and Surf.,* **39,** 127 (1989).
40. J. P. Celis, J. R. Roos, and C. Buelens, *This Journal,* **134,** 1402 (1987).
41. K. M. Gorbunova and Z. A. Tkachik, *Electrochim. Acta,* **16,** 191 (1971).
42. J. D. Reid and A. P. David, *This Journal,* **134,** 1389 (1987).
43. R. C. Bowen, D. S. Rimai, and L. P. Demejo, *J. Adhesion Sci.,* **3,** 623 (1989).
44. L. P. DeMejo, D. S. Rimai, and R. C. Bowen, in "Particles on Surfaces, 2," K. L. Mittal, editor, p. 49, Plenum Publishing Corp. (1989).
45. Y. I. Rabinovich, B. V. Derjaguin, and N. V. Churaev, *Adv. Colloid Interface Sci.,* **16,** 63 (1982).
46. R. M. Pashley and J. N. Israelachvili, *J. Coll. Int. Sci.,* **101,** 511 (1984).
47. R. M. Pashley and J. N. Israelachvili, *Ibid.,* **97,** 446 (1984).
48. R. M. Pashley and J. P. Quirk, *Coll. and Surf.,* **9,** 1 (1984).
49. N. Furakawa and T. Hayashi, "Proc. Interfinish 88," 119, Paris (1988).
50. R. Narayan and B. H. Narayana, *This Journal,* **128,** 1704 (1981).
51. M. N. Joshi and M. K. Totlani, "Proc. 2nd Nat. Conf. on Electroplating and Met. Finish.," p. 75, SAEST, Bombay (1981).
52. S. Matsumura, *Proc. AES,* **F3,** Chicago (1987).
53. T. W. Tomaszewski, L. C. Tomaszewski, and H. Brown, *Plating,* **56,** 1234 (1969).
54. J. Zahavi and H. Kerbel, *Proc. Interfinish, '80,* p. 208 Kyoto, Japan (1980).
55. D. J. O'Connor and J. V. Sanders, *J. Coll. Sci.,* **11,** 158 (1956).